Available online www.jsaer.com

***Journal of Scientific and Engineering Research*, 2021, 8(6):64-83**

Research Article

ISSN: 2394-2630
CODEN(USA): JSERBR

About the Effect on the Airfoil Wake Induced by Periodic Mobile Flap

Julio Marañón Di Leo[1,2], Juan Sebastián Delnero[1,2], Iban Echapresto Garay[1,2], Ariel Nicolás Gamarra[1], Pablo Marcelo Mantelli[1], Javier Donati[1,2]

[1]UIDET LaCLyFA/CTA: Departamento de Aeronáutica, Facultad de Ingeniería, Universidad Nacional de La Plata, La Plata, Argentina
[2]CONICET, Consejo Nacional de Investigaciones Científicas y Técnicas, Buenos Aires, Argentina

Abstract The flow in the wake of an aerodynamic airfoil gives us information about the flow pattern that generates the aerodynamic forces. This wake will depend not only on the geometry of the model, but also on the characteristics of the incident flow. If the airfoil has a flow control system, it can modify the characteristics of the resulting flow field. The wake turbulence in this case will be modified. In the near wake, it will be possible to study the mechanisms of generation and vortex shedding, while the analysis of the distant wake provides us with information on the general fluid-dynamic field resulting from the aero-dynamic forces.

The objective of the present work is to study the develop of the fluid-dynamic structures found in the NACA 4412 airfoil wake, as well as the development of the same structures when flow control techniques are applied by means of an oscillating Gurney Flap place in the lower surface of the wing model, close to the trailing edge. The flow control system was set at different frequencies. In order to study the effect of the control mechanism on the wake, hot wire anemometry techniques were used. Two components of the velocity vector were measured - longitudinal and vertical by means of a vertical array of three sensors acquiring simultaneously.

Velocity fluctuations will be analyzed, as well as turbulence intensities, integral scales and flow energy, in order to quantify the turbulent wake generated and understand the mechanisms involved in its generation.

Keywords Wind tunnel, Aerodynamic, Detachments, Re-circulatory, Hot-wire anemometry

Introduction

The use of flaps as high-lift devices brings an increase in lift, but also in resistance. Achieving further efficiency is always a big challenge. The development of active and passive flow control systems acting on the wings or flaps has opened a large field of study. This allows us to try to determine how the flow behavior is on the wings and the control devices.

Conventional flaps have robust mechanisms that can be actuated to modify the pressure distribution on it, and thus meet its objective. There are other smaller and less complex flow control or high lift devices that can also be used.

One of those high-lift devices is the so-called Gurney Flap [1]. This device was originally implemented by the American racing car driver Dan Gurney as a rear aileron in one of his cars. The Gurney flap was studied by many authors such as Liebeck [2], Neuhart and Pendergraft [3], Bloy [4] and Storms and Cory [5], reporting an increase of the lift and lift-to-drag ratio and a reduced form drag obtained at high lift coefficients compared with the same airfoil without the flap.

The wake immediately downstream a common lifting airfoil is asymmetric due to the different external and boundary layer flows on the pressure and suction surfaces of the airfoil. The wake structure in this near wake region is influenced by aero dynamical loading and airfoil characteristics.

Downstream of the trailing edge of a normal lifting airfoil the downwash diminishes rapidly. Hah and Lakshminarayana [6] in their experimental and numerical study, about the near wake of a lifting airfoil, confirmed that the asymmetric wake becomes nearly symmetric after only one chord length downstream of the trailing edge. These authors reported also that the far wake shows a roughly symmetric wake structure in which the airfoil features and aero-dynamical loading which do not influence the wake development anymore. The main downwash occurs within the asymmetric region.

The unsteady nature of the counter rotating vortices behind a Gurney flap complicates, despite a long-standing experience in the classic lift evaluation due to a vortex system bound to a wing, a physical realistic theoretical understanding of the lift increase generated by these miniflaps. It is known that the highly unsteady nature of flows associated with vortex shedding make difficult its theoretical and experimental understanding.

Giguére et al [7], described experimentally the aerodynamic behavior of these flaps scaling their height with the boundary layer thickness. These authors conjectured that the trailing edge counter-rotating vortices induce streamlines resembling a smooth aerodynamic prolongation of the airfoil, allowing a better trailing edge pressure recovery, adding a virtual camber by shifting downward the Kutta condition.

A more detailed description of the flow structures in the Gurney flap pattern obtained by experiments with laser Doppler anemometry (LDA) was reported by Jeffrey et al [1] [8].

Aspects of the behavior of airfoils equipped with miniflaps with different lengths were described in [9], reported about the influence of free stream turbulence structure on these devices.

The vortex generation and shedding mechanisms will be given by the fluid interaction between the high-lift device and the wing, in the so-called near wake. This will be developed in the far wake. These vortices are generated by the positive and negative pressure changes that occur during this process. Therefore, the incident flow characteristics should not go unnoticed. It is necessary to quantify the effect of the incident turbulence intensity, as well as the spatial and temporal scales of the turbulence, compared at equal aver-age velocities. The energy carried by the fluid will be of utmost importance in the mechanisms of generation and evolution of the flow wake of the wings.

In the near wake of a wing airfoil provided with Gurney mini-flaps, in lift conditions, the starting vortices detached from the upper surface must show a different intensity than those detached from the lower surface. The existence of the counter-rotating asymmetric vortices, in the near wake of an airfoil provided with trailing edge Gurney mini-flaps, was experimentally demonstrated [10].

Experimental results were obtained about the behavior of Gurney mini-flaps placed at the trailing edge of an airfoil, about the effect of different turbulent flows on the lift and drag coefficients, compared with a quasi-laminar flow [11]. Experiments also clarified the effect of turbulence on Gurney mini-flaps of different sizes placed at several distances from the trailing edge [12]. Similar results were found in numerical simulations compared with experimental results [9] [13].

The common fluid dynamic models of airfoils with Gurney flaps describe a change in the flow pattern resembling a camber increment and a downward shift of the external rear stagnation point.

In some studies, about aerodynamic efficiency of Gurney flaps it is common to find the assumption that the effect of the vortex wake on lift to drag ratio is detrimental. In order to attain a drag reduction by “stabilizing the wake” some authors suggest the use of span-wise holes, slits, serrated flaps and wake-bodies [14], [15], while other recommend to eliminate straightforward the double row of counter-rotating vortices of the wake be-hind a Gurney type mini-flap [16]. The combined effect of the gurney flap with vortex generators was analyzed [17].

Tests have been carried out in order to be able to quantify the interactions between the flap and the turbulent wake produced. This type of flow control device can be given by an air jet or a mobile flap at a certain frequency.

The vortex shedding produced by a lifting airfoil is connected to time variations of the bound vortex strength [18]. It is quite evident that, for an airfoil provided with Gurney mobile Flap, the vortex line shed behind the trailing edge must be also connected to the overall circulation around the airfoil. The strength of the vortices generated by the rolling up of the lower surface shear layer is connected to an augmented circulation of the bound vortex, promoting a lift increase. This cannot be counteracted by the lift decrease due to the weaker opposite circulation connected to the counter rotating rolling up shear layer detached from the upper surface.

This leads us to believe that the analysis and control of the wake of an airfoil will allow us not only to understand the mechanism of force generation, but also to quantify the effect it has on the entire fluid-dynamic field.

For all these reasons we propose to study the far wake and the near wake of an airfoil provided with Gurney mobile flap, immersed in turbulent flow. Different configurations of the model will be tested, in order to find the flow asymmetries and to explain the previously mentioned behavior and the influence of turbulence. It is important to note that there are few works studying the aerodynamic behavior and the wake structure of airfoils provided with active and/or passive flow control devices, such as Gurney mobile flap, immersed in free turbulent flow [19] [20].

The shear layers related to active Gurney mobile flap in the wake of the airfoils, depend significantly on the characteristics of the upstream free flow profile, as well as on the device oscillation frequencies. This implies the need for a more detailed measuring of the fluid dynamics wake structure, until a minimum of one chord length behind the airfoil. This is the motivation of this work.

Methodology

According to the proposed objective, we will study the turbulence structure of a wake generated by a wing model with a NACA 4412 airfoil equipped with a Gurney Movable Flap (GMF) on the upper surface and close to the trailing edge. The flap device is electromechanical. The study will be carried out by measuring the velocity field in the wake of the airfoil.

Instant velocities in three different points will be simultaneously measured with a hot wire anemometer, in order to quantify the effect of the flap on the wake. Instant and mean velocities, turbulence intensity, spatial and time scales and frequency spectra will be analyzed.

Temporal and spatial integral scales were calculated from the autocorrelation coefficients analysis (Equation 2). The autocorrelation function (Equation 1) and its coefficient (Equation 2) are defined as follows:

$$\boldsymbol{R_{u'}(\Delta t) = \lim_{T\to\infty} \frac{1}{T}\int_0^T u'(t)\cdot u'(t+\Delta t)\cdot dt} \quad (1)$$

$$\boldsymbol{C(\Delta t) = \frac{R_{u'}(\Delta t)}{\sigma^2_{u'}}} \quad (2)$$

Where $\boldsymbol{\sigma^2_{u'}}$ is the variance and is defined as

$$\boldsymbol{\sigma^2_{u'} = lim_{T\to\infty} \frac{1}{T}\int_0^T u'^2(t)\cdot dt} \quad (3)$$

The autocorrelation coefficient function takes the unity value at time t = 0, when the acquisition starts, and trends to zero when the interval of time goes to infinity.

The time gap between t = 0, and the time when the autocorrelation coefficient C(t) takes the value 1/e, for the first time, give an approximated value of the integral time scale (λt). With this scale, and the mean value of the flow component under analysis, the spatial integral turbulent scale can be calculated, using the Equation 4

$$\boldsymbol{\lambda = \bar{V}\cdot \lambda_t} \quad (4)$$

Additionally, the turbulence intensity was calculated as follows:

$$\boldsymbol{Ti_u = \frac{\sigma_{u'}}{V};\ Ti_v = \frac{\sigma_{v'}}{V}} \quad (5)$$

Facilities and Test Conditions

The model was based on a NACA 4412 airfoil and was built with a wooden, aluminum and polystyrene. This kind of structure gave enough interior space to lodge the electromechanic crank-connecting rod system, driving the aluminum made gurney flap. The engine rpm. can be varied and so the GMF oscillation frequency, up to a maximum of 30Hz. The chord length C of the model is 400mm and its span 800mm. The GMF is placed at 10%C from the trailing edge and its length is 1.5%C, as shown in Figure 1.

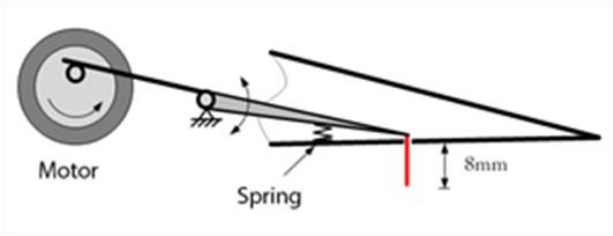

Figure 1: Electro-mechanic GMF actuation system.

The model was mounted in the wind tunnel between two panels to ensure the flow bidimensionality. A scheme is shown in Figure 2 and Figure 3. The tests were conducted in the wind tunnel of the UIDET-LaCLyFA at the National University of La Plata [21]. It is a closed-circuit wind tunnel [22], with a test section of 1.4 m x 1.0 m x 7.5 m and Vmax = 20 m/s.

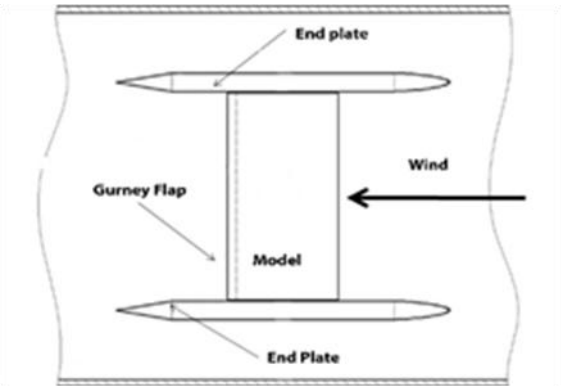

Figure 2: Wind Tunnel Setup

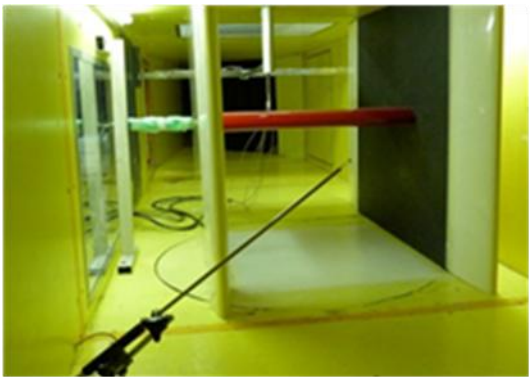

Figure 3: Wind Tunnel View

The measurement of the instantaneous velocity field was performed using a hot wire anemometry system (CTA Dantec Streamline), with a dual sensor (fiber film probes 55R51). The acquisition was made at a sample frequency of 2 kHz, using a low-pass band filter at 1 kHz, acquiring 16,384 samples in each test.

The vertical (v) and longitudinal (u) components of velocity were simultaneously measured at three points (upper, middle and lower row positions), by means of and arrange of three probes. The probes were placed at a vertical line, separated 10mm from one another (Figure 4).

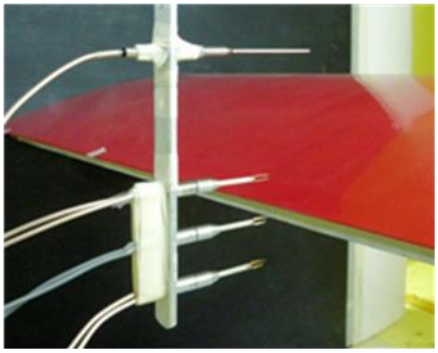

Figure 4: Hot wire anemometer probes at the wake.

In order to analyze the wake, several measurements were made placing the probe arranges at different distances downstream the trailing edge (Figure 5).

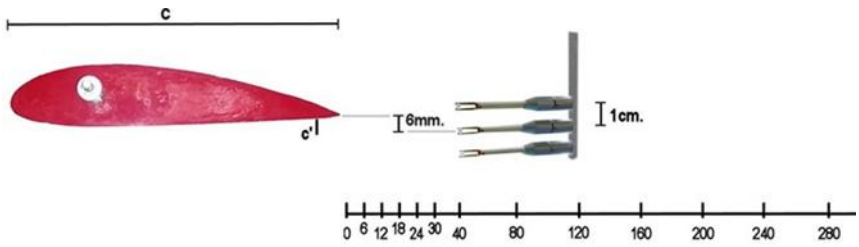

Figure 5: Measurement points (upper, middle and lower row positions)

Tests were performed at a free stream velocity of 10m/s. Two angles of attack were used, 0º and 2º. Six different configurations were tested: plain model (no GMF), fixed GMF and oscillating GMF at four different frequencies (16, 20, 25 and 30Hz). The incoming flow was found to be turbulent, and 2% turbulence intensity was calculated in the surroundings of the model.

Figure 6 shows the distribution of the turbulent intensity for the longitudinal velocity component. These results were obtained from tests carried out using hot wire anemometry techniques. The figure shows the area where the model was tested.

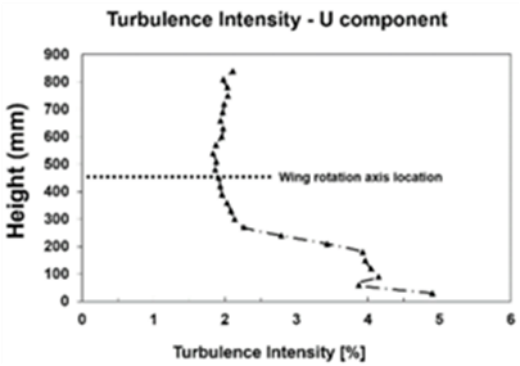

Figure 6: Vertical Distribution of the Turbulent Intensity for the longitudinal velocity component

Results

Velocity analysis

Results from the processing and analysis of the acquired data are shown by means of mean velocities, scales, intensities, and frequency spectra for the two velocity components.

Mean velocity distribution for the six configurations are plotted along the wake. Both components (u and v) are shown in the following figures.

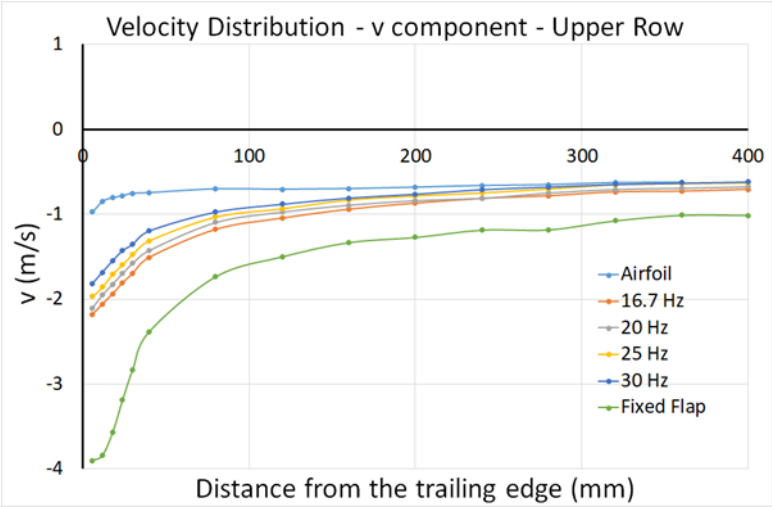

Figure 7: v mean velocity distribution–upper row-α = 0º

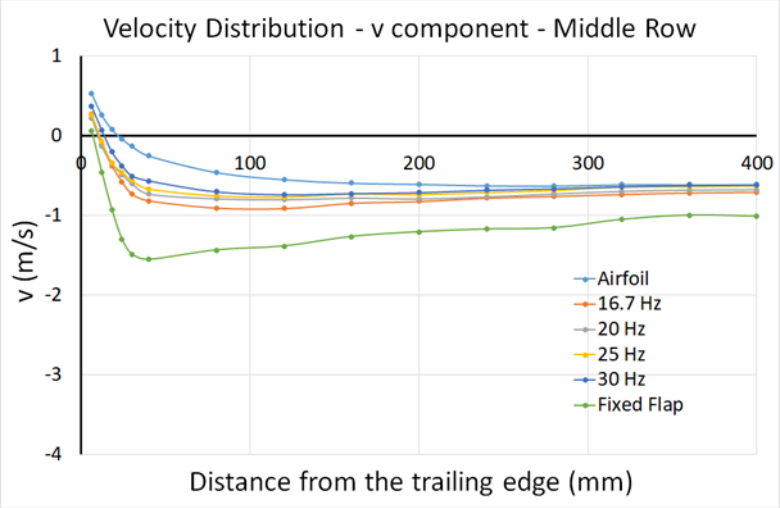

Figure 8: v mean velocity distribution-middle row-α= 0º

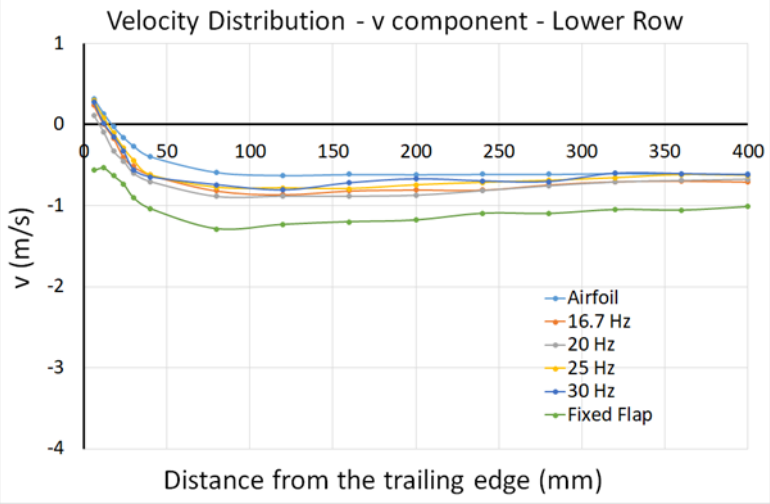

Figure 9: v mean velocity distribution-lower row-α= 0º

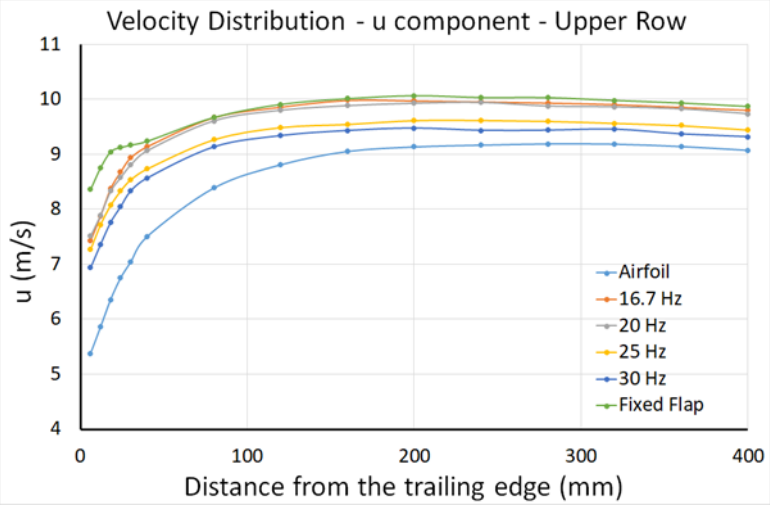

Figure 10: u mean velocity distribution–upper row-α = 0º.

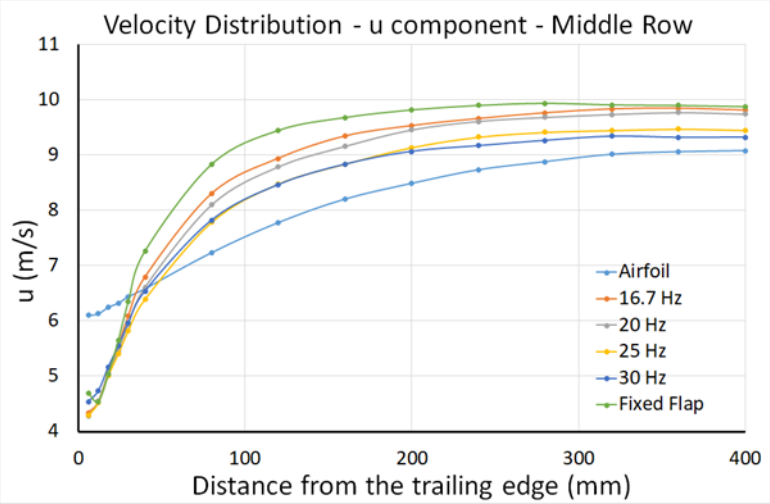

Figure 11: u mean velocity distribution–middle row-α = 0°

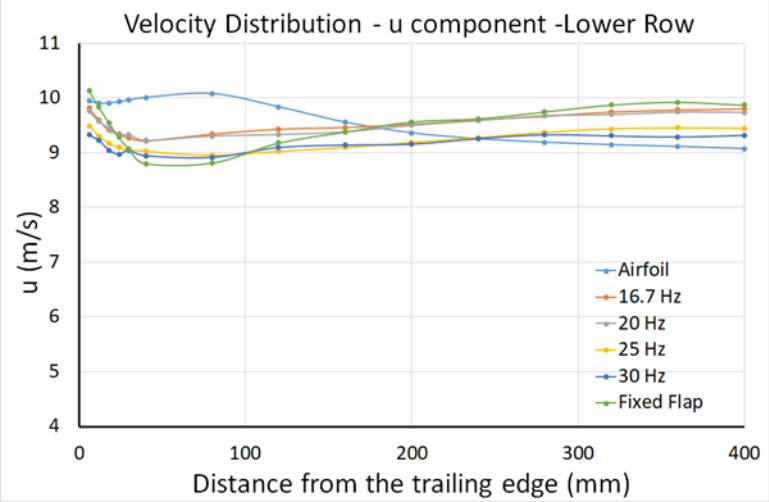

Figure 12: u mean velocity distribution–lower row-α = 0°

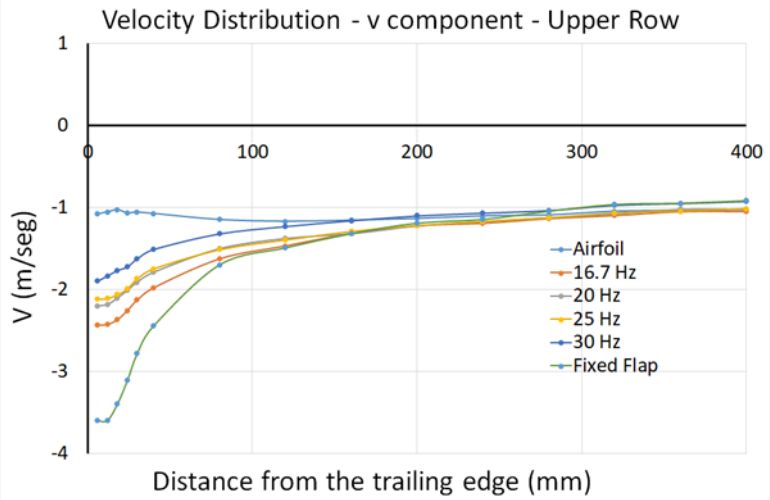

Figure 13: v mean velocity distribution–upper row-α=2°

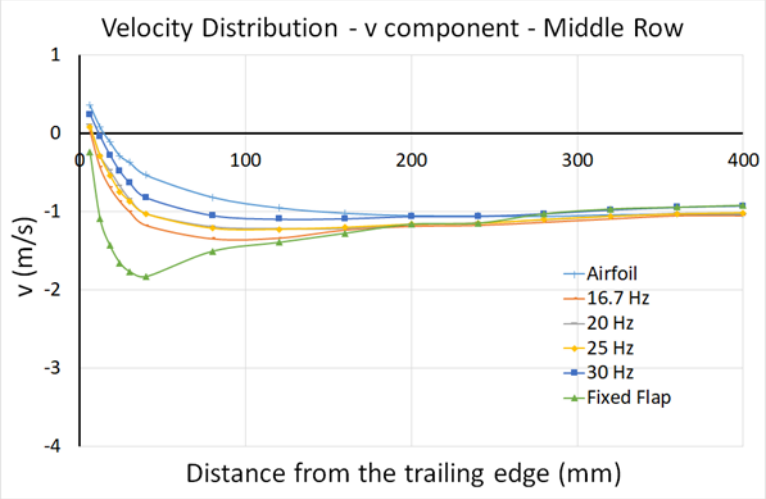

Figure 14: v mean velocity distribution–middle row-α=2º

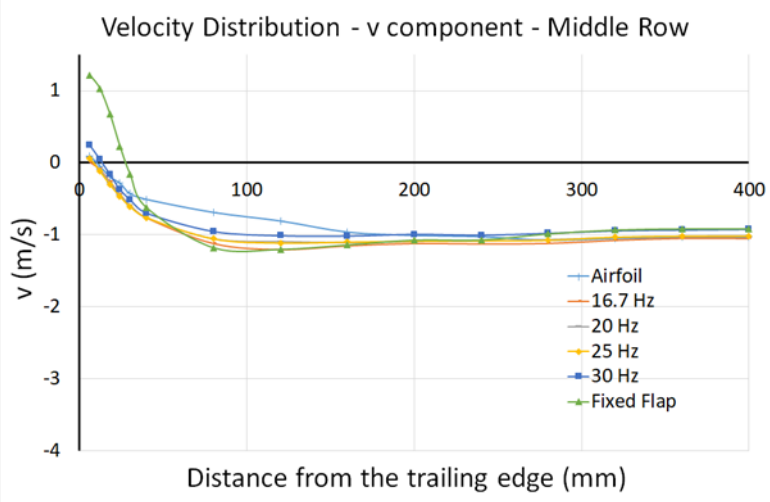

Figure 15: v mean velocity distribution–lower row-α=2º

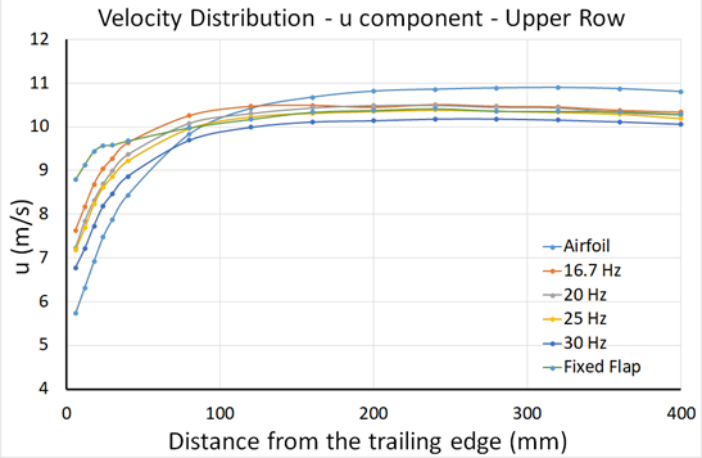

Figure 16: u mean velocity distribution–upper row-α=2º

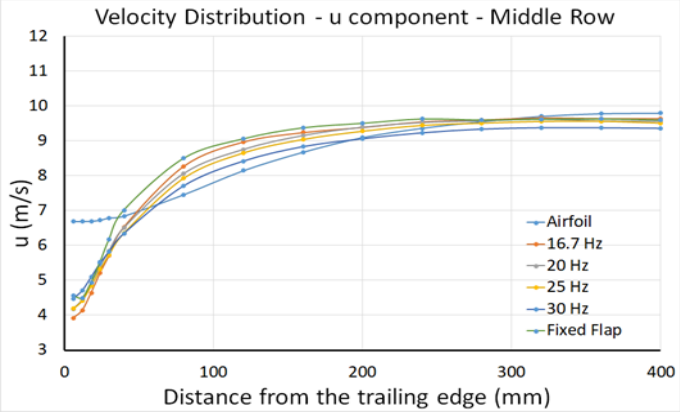

Figure 17: u mean velocity distribution–middle row-α=2º

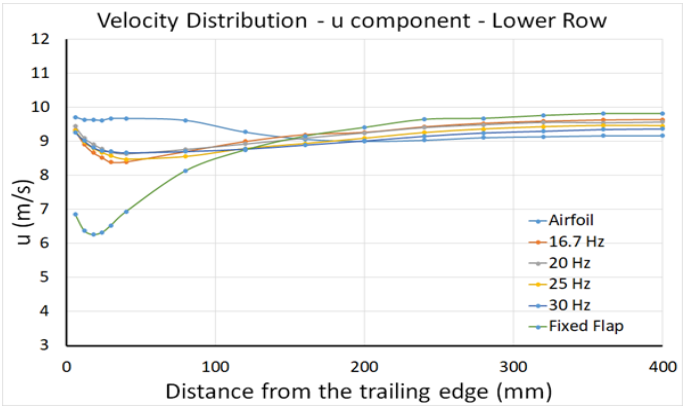

Figure 18: u mean velocity distribution–lower row-α=2º

In order to find a relationship between the effect of the flap on the wake, the instantaneous velocities in the longitudinal (u) and vertical (v) components are plotted for different points in the airfoil wake. This distribution is divided into two zones called the near wake (corresponding to less than 10% chord behind the trailing edge) and the far wake (up to 100% of the chord). All these results will be analyzed for two angles of attack (0 and 2 degrees). Three positions are shown in the plots corresponding to the simultaneous sensors measuring the velocities (named as upper, middle and lower row).

The u-component is seen to increase in all configurations as measured farther from the trailing edge. However, the greatest changes are observed in the v-component, showing different behaviors in the plain airfoil, in the fixed GMF and in the oscillating GMF. The fixed GMF generates the greatest vertical velocities, thus, the greatest downwash, being responsible for the lift and drag increases. The oscillating GMF generates higher downwash in the far wake, while the plain airfoil generates downwash in the near wake. The behavior did not show remarkable differences related to the oscillation frequencies.

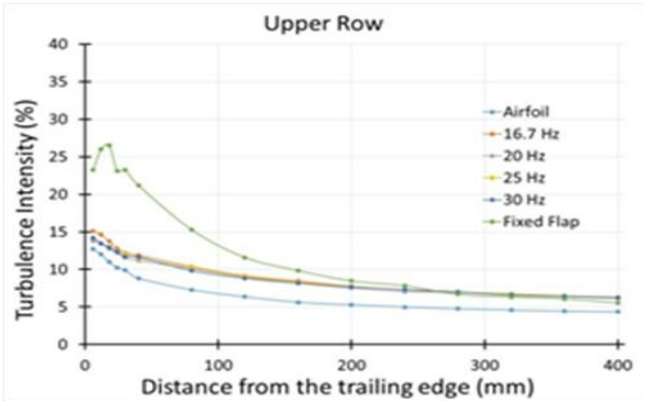

Figure 19: Turbulence Intensity - α = 0º

According to the (Eq. 5), the v component velocity turbulence intensity distributions are calculated for the near and far fields at the six different test conditions. Results are plotted in Figures 19-24.

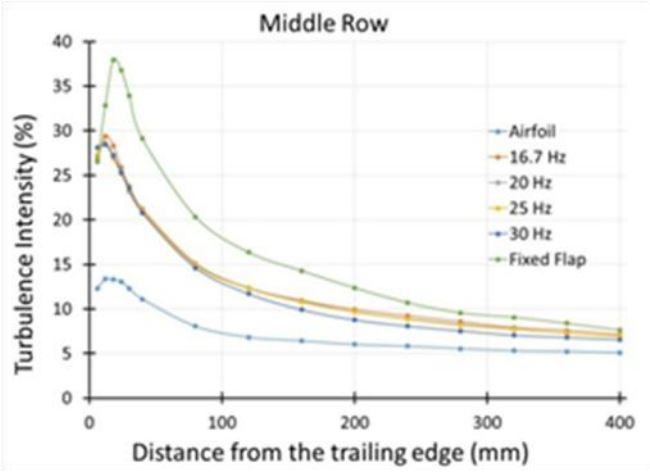

Figure 20: Turbulence Intensity - $\alpha = 0^o$

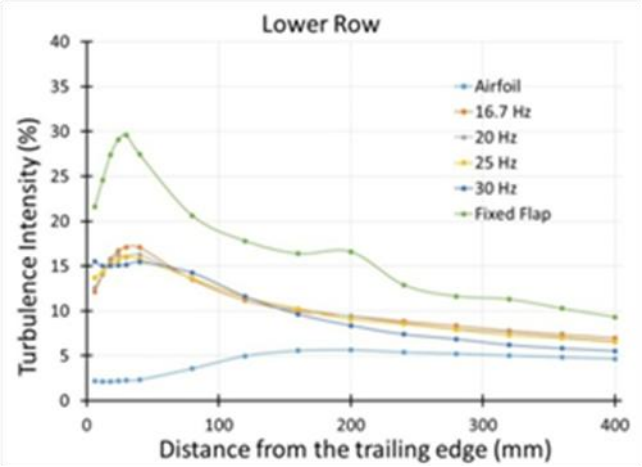

Figure 21: Turbulence Intensity - $\alpha = 0^o$

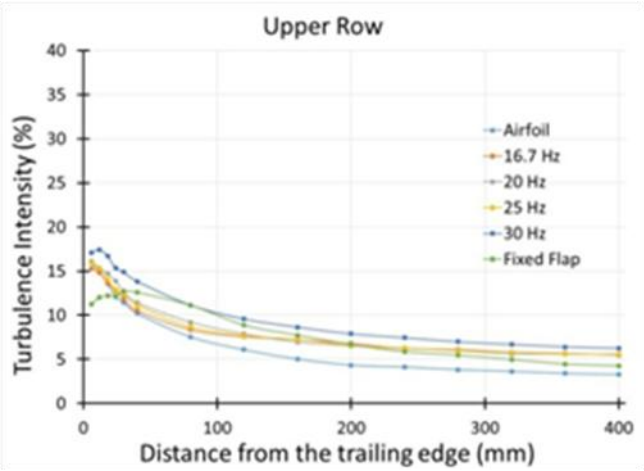

Figure 22: Turbulence Intensity - $\alpha = 2^o$

In all cases the turbulence intensity values diminish and converge to a unique value in the far wake. In the configurations with oscillating GMF the slope is more pronounced that in the fixed device. The wake produced by the oscillating configurations is less turbulent than the one produced by the fixed flap. Again, no remarkable differences are shown due to the oscillation frequency.

For the case of 2 ° it can be observed. When the angle of attack is increased a slight decrease is observed in the near wake. In the far wake the behavior remains unaltered and its value is practically constant.

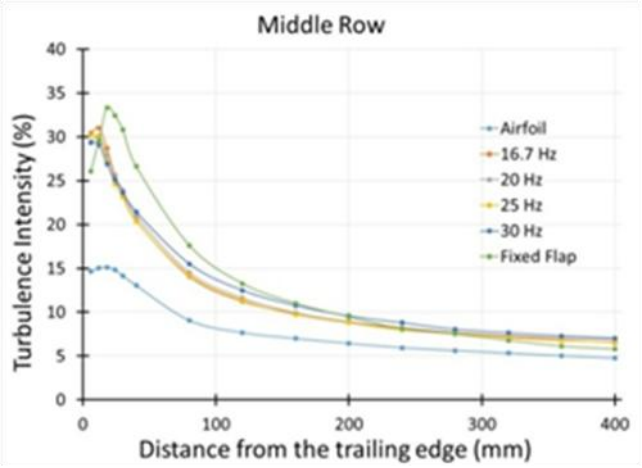

Figure 23: Turbulence Intensity - α = 2º

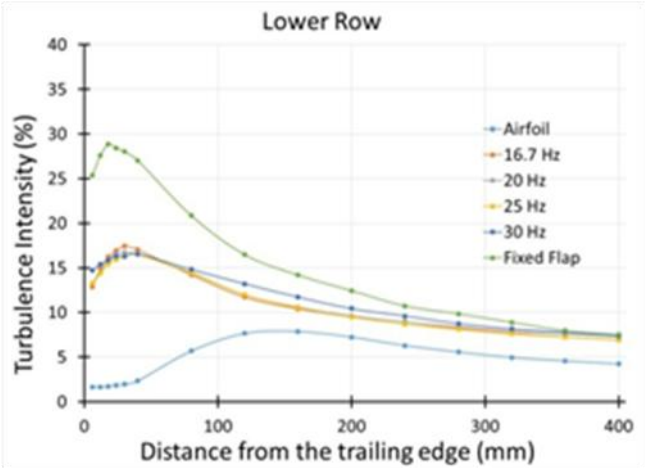

Figure 24: Turbulence Intensity - α = 2º

Autocorrelation Analysis

The spatial integral turbulent scales were determined from autocorrelations results and applying frozen flow theory [21]. The distribution of the autocorrelation function at null angle of attack is shown for both fields and for the different oscillation frequencies, in Figure 25 and Figure 26. From the distribution of the autocorrelation function, it is found that all of them are periodical. In the still GMF case the oscillation frequency produced by the vortex shedding is found. In the same way, for the oscillating GMF cases it is seen that the forcing frequency is imposed. As expected, the shedding frequency is more intense in the near field.

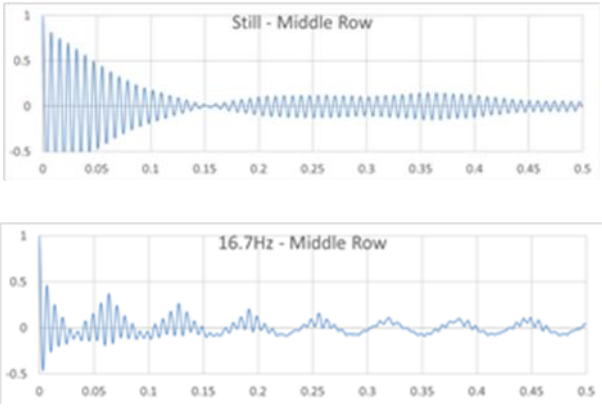

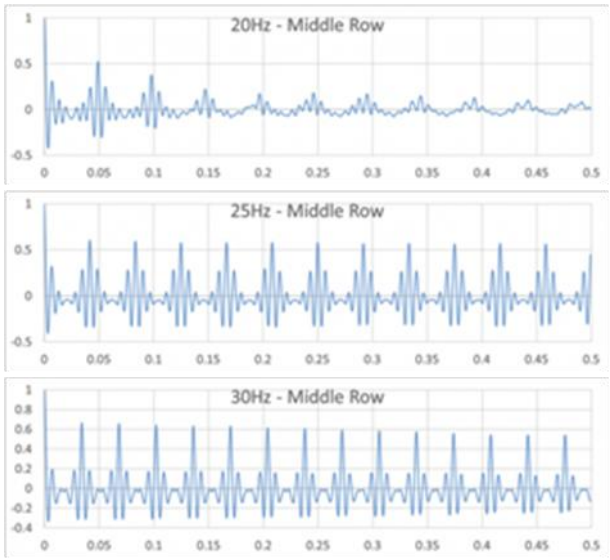

Figure 25: Autocorrelation Distribution Coefficients - Near field

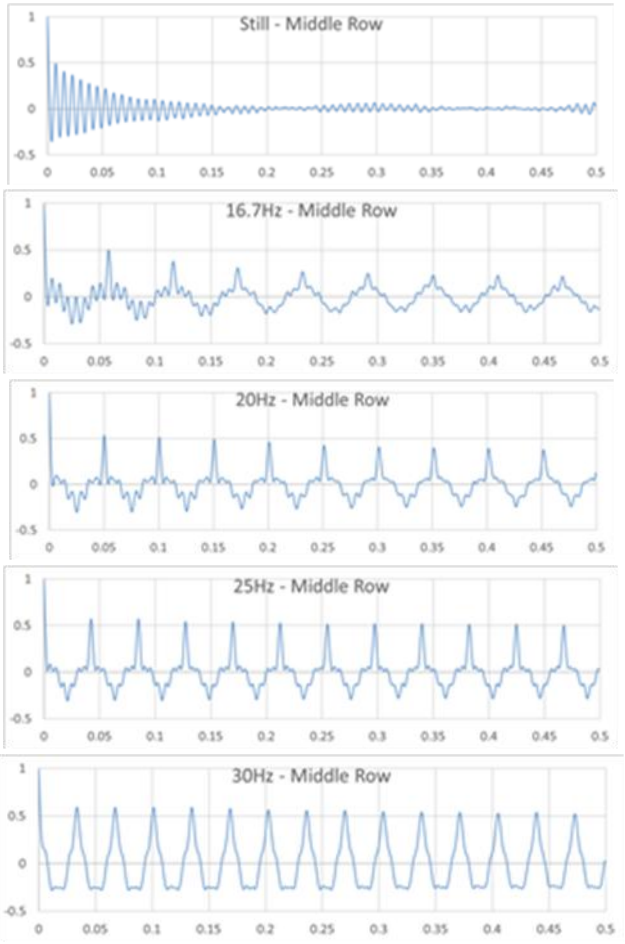

Figure 26: Autocorrelation Distribution Coefficients - Far field

The results are similar according to the analysis of the autocorrelation functions at different points in the wake. Figure 25 only shows a particular point in the near wake. In any case, all the values of the spatial and temporal scales in the wake will be determined using the autocorrelation functions, as shown below.

Applying the frozen flow theory, combined with the exponential decay criteria, the temporal and spatial turbulent scales are determined for both velocity components.

Figure 27 shows the turbulent time scales (u-component) at different positions of the wake for the three sensors, in the cases of the airfoil, the fixed gurney flap and the mobile flap at a frequency of 25 Hz.
Since the behavior is similar for the different frequencies, we will take only one frequency in order to observe the graphs in more detail. Using the same frozen flow theory. The values for three configurations, plain airfoil, still GMF and 25Hz frequency – the other frequencies show similar results.

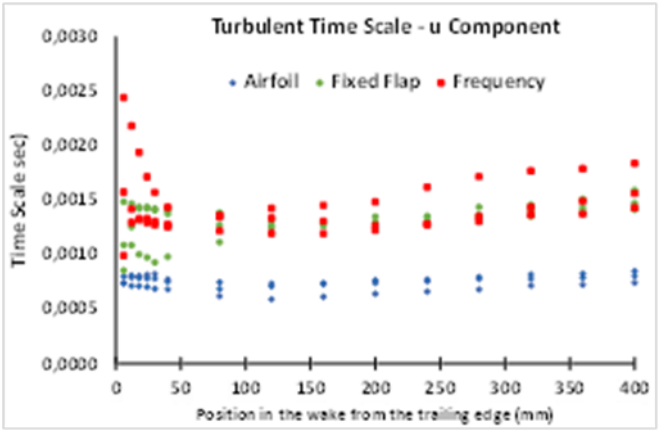

Figure 27: Turbulent time scale – u component.

It is observed that the turbulent time scales of the airfoil wake are constant throughout it and of lower value than the other cases. For the fixed and mobile gurney cases, a random behavior is observed in the near wake. Slightly increasing values are observed in the far wake. The near wake is considered to develop at a distance of 30 mm
In all cases it is seen that the scales are larger at the far wake. In the still GMF configuration and oscillating GMF configurations the scales are very similar. The airfoil generates the smallest turbulent time scales.
For the airfoil, it is observed that the sensors placed in the upper row, middle row and lower row acquire values that give constant turbulent time scales throughout the wake.
Figures 28, 29 and 30 show the turbulent spatial scale obtained from the time scales and mean velocities. They are plotted for the three sensors in the airfoil cases, the fixed gurney and the mobile gurney at a frequency of 25 Hz.

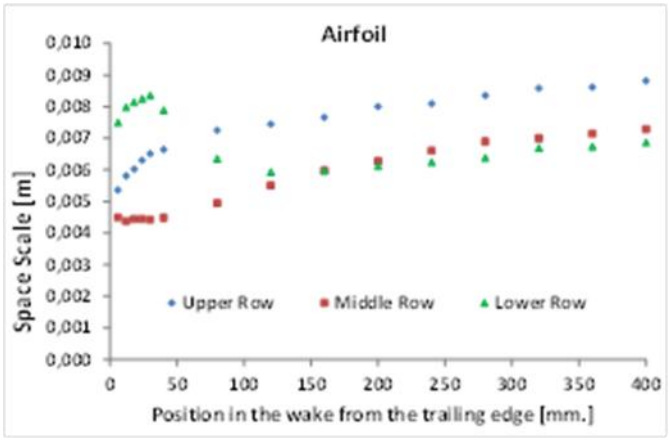

Figure 28: Spatial Scale – Airfoil

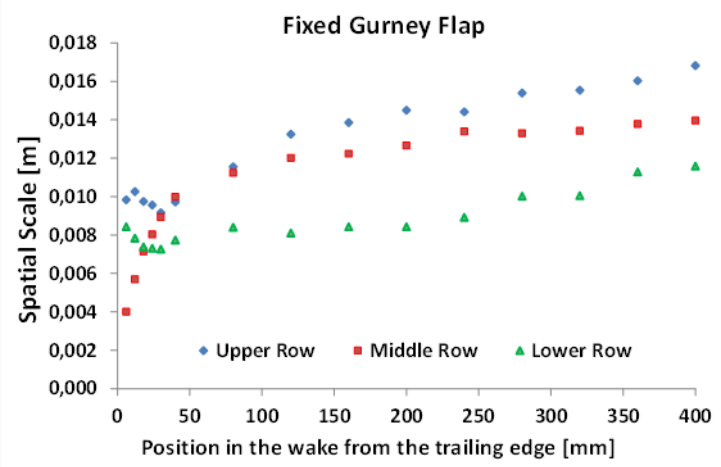

Figure 29: Spatial Scale -Fixed gurney flap.

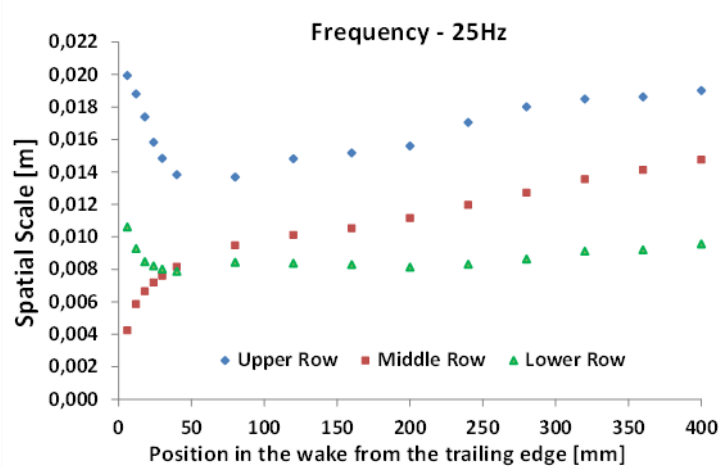

Figure 30: Spatial Scale -gurney flap at frequency 25 Hz

Evidence of chaotic flow characteristics is found from both, temporal and spatial scales in the near wake. This is due to the velocities and intensities induced by the vortices generated in that area. In all figures, the behavior of the flow is clearly observed in the so-called near wake. Then, the flow develops during the far wake. In all cases there is an increase in spatial scales as we move away from the trailing edge of the airfoil, as expected.

Figure 31 shows the turbulent spatial scale for the different cases. The sensor placed in the middle row is analyzed. It is observed how the scales develop along the wake. The values of the scales obtained from the fixed gurney and the mobile gurney are greater than the airfoil. Near the trailing edge of the airfoil, they are all similar.

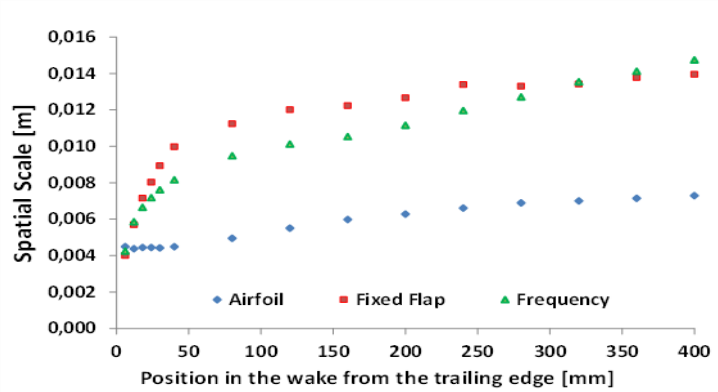

Figure 31: Turbulent Spatial Scale at middle row sensor

A larger difference can be observed in the case of the scales corresponding to the mobile flap compared to the fixed or the airfoil alone.

PSD Analysis

Power Spectral Density (PSD) of the signals was determined for the different frequencies and for the different configurations. The two components of the signal were analyzed, plotted (shown in Figures 32, 33 and 34) and tabulated (shown in Tables 1, 2 and 3) to facilitate their study. Results for the three previously mentioned configurations are shown. In all cases, for comparative reasons, the plot representing the near wake (3%C) and the plot representing the far wake (100%C) are shown side by side; while each row represents the position of the represented probe (upper, middle and lower).

The PSD peak indicates the relative amount of energy associated with the vortex structures traveling in the wake and their dominant frequency.

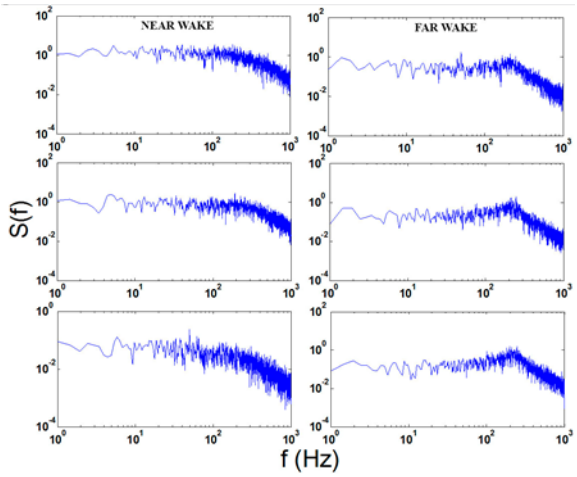

Figure 32: PSD – Airfoil

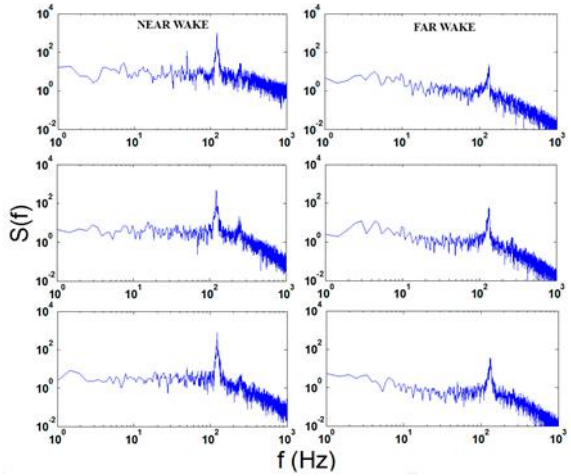

Figure 33: PSD – Fixed Gurney Flap

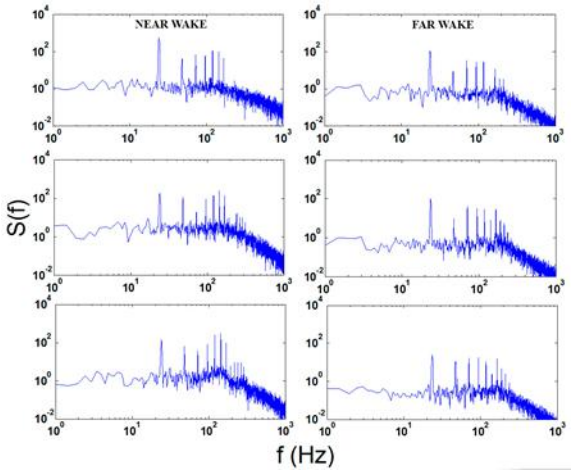

Figure 34: PSD – Frequency 25 Hz

From the PSD general analysis an increment of power due to the introduction of the GMF – oscillating or still – is observed. Energy peaks are observed in both configurations provided with GMF, while none is observed in the plane airfoil configuration. As expected, in all cases the energy diminishes along the wake as the measure is taken farther from the trailing edge. The detachment of asymmetric, counter-rotating, periodical vortices shed by the still GMF shows such energy decrease along the wake keeping its frequency unaltered. Its effect in the near wake and in the far wake is very strong. In the oscillating GMF wake, several peaks are detected coinciding the forcing frequency to the largest one. The rest of the peaks correspond to harmonics of the acquired signal.

In general, is seen that in the near wake the vortices corresponding to the still GMF are more energetic that those shed by the oscillating GMF. In the far wake the vortices and perturbations generated by the oscillating GMF remains more energetic along the wake than those generated by the still GMF, which decay sooner. The forcing energy introduced with the oscillating GMF seems to be responsible for that effect.

No appreciable changes are observed in the plain GMF wake energy; except for a small distortion, most likely provoked by a flow instability.

Table 1 to Table 3 show the reference values and energy values in all the field.

Table 1: PSD values for airfoil.

Distance from TE	**mm.**	**6**	**12**	**18**	**24**	**30**	**40**	**80**
Upper row	**f (Hz)**	155.8	183.6	162.6	50.78	6.348	117.7	191.9
	S(f)	4.657	3.693	3.437	3.445	3.478	2.542	2.718
Middle row	**f (Hz)**	33.69	190.4	23.44	18.55	33.2	174.8	212.4
	S(f)	1.985	2.849	3.232	2.663	2.253	2.494	2.346
Lower row	**f (Hz)**	43.46	49.8	0.9776	49.8	49.8	49.8	49.8
	S(f)	0.1068	0.2328	0.2367	0.2958	0.4644	0.8061	0.7271
Distance from TE	**120**	**160**	**200**	**240**	**280**	**320**	**360**	**400**
Upper row	151.4	235.8	49.8	219.7	219.9	238.8	211.4	49.8
	1.869	1.942	1.728	1.492	1.784	1.38	1.403	1.723
Middle row	187.5	247.1	175.3	206.5	223.6	228.5	211.4	247.1
	2.415	2.417	2.198	1.979	2.064	2.082	2.276	1.973
Lower row	187.5	247.1	243.7	233.4	243.7	228.5	211.4	197.8
	0.8511	1.165	1.241	1.85	1.663	1.784	1.873	1.527

Table 2: PSD values for fixed Gurney flap at 96% chord length

Distance from TE	mm.	6	12	18	24	30	40	80
Upper row	f(Hz)	24.41	23.93	23.93	23.93	23.93	23.93	23.93
	S(f)	578.2	572.5	495.2	370	360.7	256	146.6
Middle row	f(Hz)	24.41	23.93	23.93	23.93	23.93	23.93	23.93
	S(f)	91.81	184.9	224.7	211.7	234.1	266.8	148.9
Lower row	f(Hz)	24.41	23.93	23.93	23.93	23.93	23.93	23.93
	S(f)	213.4	143.6	79.8	56.83	61.75	96.88	118.9
Distance from TE	**120**	**160**	**200**	**240**	**280**	**320**	**360**	**400**
Upper row		23.93	23.93	23.93	23.93	23.93	23.93	23.93	23.44
		168.8	150.5	17.4	141.6	128.7	120.2	125.5	108.7
Middle row		23.93	23.93	23.93	23.93	23.93	23.93	23.93	23.44
		138.1	113.3	91.78	113.5	108.6	108	119.8	107
Lower row		23.93	23.93	23.93	23.93	23.93	23.93	23.93	23.44
		82.36	49.22	33.7	29.05	28.03	29.59	22.56	24.55

Table 3: PSD values for oscillating Gurney flap a frequency 25Hz

Distance from TE	mm.	6	12	18	24	30	40	80
Upper row	f(Hz)	120.6	122.6	127	125.5	126.5	128.9	129.4
	S(f)	620.2	977.2	820.6	787.8	750.2	532.8	360
Middle row	f(Hz)	120.6	122.6	122.6	125.5	126.5	128.9	129.4
	S(f)	71.66	484.2	838.8	1422	1562	1240	893.3
Lower row	f(Hz)	120.6	122.6	126.5	125.5	126.5	128.9	129.4
	S(f)	650.7	786	463.9	663.2	745.8	531.8	436.7
Distance from TE	**120**	**160**	**200**	**240**	**280**	**320**	**360**	**400**
Upper row		131.8	134.8	130.9	130.9	130.9	134.3	133.8	132.8
		171.9	160.2	81.19	65.21	37.21	49.84	25.77	23.85
Middle row		131.8	134.8	130.9	133.8	130.9	134.3	134.3	132.8
		436.3	391.2	186.4	158.6	110.7	153.3	69.76	60.2
Lower row		132.3	134.8	130.9	133.8	130.4	134.3	133.8	130.9
		186.9	213.1	103.7	80.86	57.16	90.4	46.12	36.21

Discussion

The introduction of the still flap in the airfoil is responsible for the increment in lift and drag forces [11] [8]. This is due to the generation of flow instabilities by the shed of counter-rotating, asymmetric vortices [10]. It was also proved that the GMF performance changed when submitted to flows with different turbulence characteristics [12]. The questions arising now are: How dependent on the turbulence in the wake is the behavior of the airfoil provided with oscillating GMF? The efficiency of the airfoil is improved as the wake becomes more turbulent? Is more downwash generated? Is it possible that the vortex generation mechanism in the wake is influenced by the vortex energy of different scales of the incident flow?

The analysis of the instant velocity components for the different configurations, regarding their directions and intensities, analyzed together with the behavior of the model at the different flow conditions, may offer a good approach to the answer. See Figure 7 to Figure 18.

From the turbulence intensity, time scales and spatial scales analysis the airfoil wake, with or without the flow control devices, is flow-dynamically characterized.

Absolute flow instabilities could be found in laminar and turbulent flow by strong peaks in the PSD charts, as it is shown in Figure 32, Figure 33 y Figure 34, for the fixed Gurney flap vortex shedding.

Values presented in Table 1 validate the hypothesis about nearfield upper and lower vortex strength differences as a mechanism capable of generating extra lift. It is assumed that PSD peaks take place in that zone where vortices start to growth and detach starting their movement into the wake.

It can also be observed in the values of the PSD tables how is the evolution of the energy of the fluid along the wake. These values should be correlated with the spatial scales and turbulence intensities to characterize the airfoil wake.

If we observe in detail the near wake, where the flow is more chaotic due to the generation of the vortices. The intermittent vortex shedding at Gurney flap upper end have been reported at reference [23], interpreted as a perturbation mechanism acting upon the shear layer coming from the wing section upper surface close to its instantaneous separation point. Therefore, the wing section lower surface shear layer separation takes place under different condition compared to that of the baseline wing section, leading to an asymmetrical vortex shedding in the vertical plane.

According to near field wake results presented in this work, it is possible to think that asymmetrical counter-rotating vortex generated by the fixed Gurney flap at the trailing edge are the mechanism that led to lift enhanced. Also, these turbulent flow case results suggest the presence of the same effect reported in laminar flow cases at the same Reynolds number.

According to the results obtained on the far wake, we can observe from the analysis of the velocities, turbulence intensities, spatial and temporal scales, as well as the PSD, that there are appreciable differences between the cases of the airfoil without flap, the airfoil with the fixed flap and the moving flap at different frequencies. It can be said that the devices affect the turbulent wake in the different cases.

Conclusions

According to the objective of this work tests were con-ducted, results were processed and analyzed in order to fluid-dynamically characterize the wake flow and its possible impact on the efficiency of the airfoil provided with an active flow control system.

The wake behind a 2D wing provided by Gurney flap under turbulent flow could be divided into two zones. The near field wake extents from the wing trailing edge up to 10% wing chord downstream. From that point on, the far field wake takes place.

A periodical detachment of vortices phenomena develops in the near field of the wake, producing an asymmetrical vortex shedding between the upper and the lower trailing edge surfaces which increase the downwash. The wake stabilizes while the spatial turbulent scales increase as it moves beyond 50% wing chord length. In the oscillating Gurney flap case, the energy of the wake does not have a well define behavior, in contrast to the clear energy decay observed in fixed Gurney flap condition.

The appearance of the asymmetric counter rotating vortices in still GMF wake, and their frequency of detachment is a consequence of the variation of the pressure in that area and of the movement of the stagnation point. All this generates the characterized turbulent wake. In the case of the oscillating GMF the pressure variation is different, since the movement of the stag-nation point is different and depend on the incoming flow, on the geometric characteristics of the GMF and on its relative position on the airfoil. In this case, as shown in [9], the vortices generated their present different intensities and scales. This, together with the incoming flow, results in wake with less turbulence intensity than for the still GMF. It would be interesting to make the GMF oscillate at a frequency like the detachment frequency since, in this manner, it would be possible to recognize the effect. When the frequency is lower, as in our experiment, several vortices are detached during the GMF movement instead of only one, as would be the ideal situation.

In the near wake area, analyzing the vertical velocities, it can be observed that the fixed flap generates more deflection of the flow stream, so there should be more downwash and therefore variation in the distribution of pressures resulting in lift and drag. The movable flap generates more vertical velocities, therefore more downwash than the case of the airfoil alone. No significant difference is observed between the different frequencies.

A similar behavior is observed in the turbulence intensities of the airfoil wake for the different cases studied. Therefore, we can affirm that the turbulent wake is altered by the oscillation of the moving Gurney flap at

different frequencies, which causes variations in the downwash and, thus, influences the aerodynamic coefficients.

Further work is needed to quantify how the wake is modified by different turbulent incident flows and their impact on the aerodynamic forces generated on the airfoil.

Acknowledgements

This work is supported by CONICET (Consejo Nacional de InvestigacionesCientíficas y Técnicas, Argentina – Technical and Scientific Research National Council).

References

[1]. Jeffrey, D.R.M. and Hurst, D.W. (1996) Aerodynamics of the Gurney Flap. *AIAA Applied Aerodynamic Conference*, AIAA 96-2418-CP.

[2]. Liebeck, R.H. (1978) Design of subsonic airfoils for high lift. *Journal of Aircraft*, 15(9), 547-561.https://doi.org/10.2514/3.58406

[3]. Neuhart D.H. and Pendergraft, O.C. (1988) A water tunnel study of Gurney flaps, NASA TM-4071.

[4]. Bloy, A.W. (1995) Aerodynamic Characteristics of an aerofoil with Small Trailing Edge Flaps. *Wind Engineering*, 19(3), 167-172. https://www.jstor.org/stable/43749576

[5]. Storms, B.L. and Cory, S.J. (1994) Lift Enhancement of an Airfoil Using a Gurney Flap and Vortex Generators. *Journal of Aircraft*, 31(3), 542-547. https://doi.org/10.2514/3.46528

[6]. Hah, C. and Lakshminarayana, B. (1982) Measurement and prediction of mean velocity and turbulence structure in the near wake of an airfoil. *Journal of. Fluid Mechanics*, 115, 251-282. https://doi.org/10.1017/S0022112082000743

[7]. Giguére, P., Lemay, J. and Dumas, G. (1995) Gurney Flap Effects and Scaling for Low-Speed Airfoils. *13th AIAA Applied Aerodynamics Conference*, San Diego, 1995. 95-1881

[8]. Jeffrey, D., Zhang, X. and Hurst, D.W. (2000) Aerodynamics of Gurney Flaps on a Single-Element High-Lift Wing. *Journal of Aircraft*, 37, 295-301. https://doi.org/10.2514/2.2593

[9]. Wassen, E., Günther, B. Thiele. F., Delnero J.S., Marañón Di Leo J., Boldes U., Colman J., Bacchi F. and Martínez, M.A. (2007) A Combined Numerical and Experimental Study of Mini-Flaps at Varying Positions on an Airfoils. *45th AIAA Aerospace Sciences Meeting and Exhibit*, Reno, 8-11 January 2007. ISBN: 978-1-62410-012-3

[10]. Boldes, U., Delnero, J.S., Marañón Di Leo, J., Colman, J. and Camocardi, M. (2010) The wake asymmetry of an airfoil with a Gurney flap and their connection with the observed lift increase. *International Review of Aerospace Engineering*, 3(2), 89-95 (2010). ISSN: 1973-7459.

[11]. Colman, J., Marañón Di Leo, J., Delnero, J.S., Martínez, M., Boldes, U. and Bacchi, F. (2008) Lift and Drag Coefficients Behaviour at Low Reynolds Number in an Airfoil with Miniflap Gurney Submitted to a Turbulent Flow. Part1. *Latin American Applied Research*. 38(3), 195-200.

[12]. Colman, J., Marañón Di Leo, J., Delnero, S., Martínez, M., Boldes, U. and Bacchi, F. (2010) Lift and Drag Coefficients Behaviour at Low Reynolds Number in an Airfoil with Miniflap Gurney Submitted to a Turbulent Flow. Part 2. *Latin American Applied Research*, 40(1), 75-80.

[13]. Casper, M., Scholz, P., Colman, J., Marañón Di Leo, J., Delnero, J. and Camocardi, M. (2012) Comparison of aerodynamic effects promoted by mechanical and fluidic miniflaps. In Colman, J. Ed., *Applied Aerodynamics*. Intech Open Access Publishers, 43-62.

[14]. van Dam, C.P., Yen, D.T. and Vijgen, P.M.H.W. (1999) Gurney Flap Experiments on Airfoil and Wings. *Journal of Aircraft*, 36(2), 484-486. https://doi.org/10.2514/2.2461

[15]. Bechert, D.W., Meyer, R. and Hage, W. (2000) Drag Reduction of Airfoils with Miniflaps. Can We Learn From Dragonflies?. *Fluids 2000 Conference and Exhibit*, 19-22 June 2000, Denver, USA. AIAA-2000-2315. https://doi.org/10.2514/6.2000-2315

[16]. Schatz, M., Guenther, B. and Thiele, F. (2004) Computational Modeling of the Unsteady Wake behind Gurney-Flaps. *2nd AIAA Flow Control Conference*, 28 June-01 July 2004, Portland, Oregon, USA. AIAA-2417. https://doi.org/10.2514/6.2004-2417

[17]. Chandra, S. and Tyagi, R. (2020) Study of Eppler 423 Airfoil with Gurney Flap and Vortex Generators. *Advances in Aerospace Science and Technology*, 5(1), 1-19. https://doi.org/10.4236/aast.2020.51001

[18]. Bertin, J.J. and Smith, M.S. (2009) Aerodynamics for Engineers. 5th Edition. Prentice Hall, Upper Saddle River, New Jersey, USA.

[19]. Gad-el-Hak M. (1998) Frontiers of Flow Control. In Gad-el-Hak M., Pollard A. Eds. Flow Control. Lecture Notes in Physics (New Series m: Monographs), 53. Springer, Berlin, Heidelberg. https://doi.org/10.1007/3-540-69672-5_2

[20]. Gad-el-Hak, M. (2001) Flow control: The future. *Journal of Aircraft*, 38(3), 402-418. https://doi.org/10.2514/2.2796

[21]. Delnero, J.S., Marañón Di Leo, J., Bacchi, F., Colman, J. and Boldes, U. (2005) Experimental determination of the influence of turbulent scale on the lift and drag coefficients of low Reynolds number airfoils. *Latin American Applied Research*. 35(3), 183-188.

[22]. Barlow, J.B., Rae, W.H. and Pope, A. (1999) Low Speed Wind Tunnel Testing. 2nd Ed., John Wiley & Sons, New York.

[23]. Troolin D.R., Longmire E.K. and Lai, W.T. (2006) Time resolved PIV analysis of flow over a NACA 0015 airfoil with Gurney flap. *Experiments in Fluids*, 41, 241–254. https://doi.org/10.1007/s00348-006-0143-8